Journal of Power Sources 184 (2008) 276–283

Contents lists available at ScienceDirect

Journal of Power Sources

journal homepage: www.elsevier.com/locate/jpowsour

Effect of $Co_3(PO_4)_2$ coating on $Li[Co_{0.1}Ni_{0.15}Li_{0.2}Mn_{0.55}]O_2$ cathode material for lithium rechargeable batteries

Sang Hyo Lee[a], Bon Keup Koo[b], Jin-Chul Kim[c], Kwang Man Kim[a,*]

[a] Energy Conversion Devices Team, Electronics and Telecommunications Research Institute (ETRI), 161 Gajong, Yusong, Daejon 305-700, South Korea
[b] Department of Materials Engineering, Hanbat National University, San 16-1, Dukmyung, Yusong, Daejon 305-719, South Korea
[c] School of Biotechnology and Bioengineering and Institute of Bioscience and Biotechnology, Kangwon National University, 192-1 Hyoja 2, Chunchon, Kangwon 200-701, South Korea

ARTICLE INFO

Article history:
Received 10 March 2008
Received in revised form 9 May 2008
Accepted 26 May 2008
Available online 22 June 2008

Keywords:
Cathode materials
Rechargeable lithium batteries
$Co_3(PO_4)_2$ coating
Cycle performance
Rate capability

ABSTRACT

To prepare a high-capacity cathode material with improved electrochemical performance for lithium rechargeable batteries, $Co_3(PO_4)_2$ nanoparticles are coated on the surface of powdered $Li[Co_{0.1}Ni_{0.15}Li_{0.2}Mn_{0.55}]O_2$, which is synthesized by a simple combustion method. The coated powder prepared under proper conditions for $Co_3(PO_4)_2$ content and annealing temperature shows an optimum coating layer that consists of a Li_xCoPO_4 phase formed by reaction with lithium impurities during heat treatment. A sample coated with 3 wt.% $Co_3(PO_4)_2$ and annealed at 800 °C proves to be the best in terms of specific capacity, cycle performance and rate capability. Thermal stability is also enhanced by the coating, as demonstrated a decrease in the onset temperature and/or the heat generated during thermal runaway.

1. Introduction

Recent progress in portable electronics, such as cellular phones, notebook computers, and devices for digital multi-media broadcasting (DMB) and wireless broadband internet (WiBro), has created a strong demand for rechargeable lithium batteries with high performance and improved safety. Because of this, in the study of cathode materials for lithium rechargeable batteries, conventional $LiCoO_2$ is beginning to be replaced by Li(Co–Ni–Mn)O_2 to ensure high capacity, high power and improved safety. The cathode material Li(Co–Ni–Mn)O_2 has in general a theoretical capacity of 277 mAh g^{-1}, a practical capacity of 135–180 mAh g^{-1}, a nominal operating voltage of 3.8 V (vs. Li/Li^+), and high thermal stability. The specific cathode material $Li[Co_{0.1}Ni_{0.15}Li_{0.2}Mn_{0.55}]O_2$, which is prepared by a simple combustion method, is known as a promising Mn-based layered oxide cathode material for providing high discharge capacity and stable cycle-life [1], and even in improving thermally aged electrochemical properties [2]. The $Li[Co_{0.1}Ni_{0.15}Li_{0.2}Mn_{0.55}]O_2$ nearly corresponds to $x = 0.2$ in the cathode material $(1-x)Li[Ni_{0.20}Li_{0.20}Mn_{0.60}]O_2$–$xLi[Co_{0.50}Li_{0.167}Mn_{0.333}]O_2$ [1].

On the other hand, metal oxide coating of the active mass of $LiCoO_2$ or Li(Co–Ni–Mn)O_2 has been examined as a means of preventing overcharge abuse and to provide stability of the respective lattice crystal structures. For instance, a coating of nanoparticle metal oxides, such as ZrO_2 [3], TiO_2 [3,4], Al_2O_3 [5,6] or $AlPO_4$ [7–9], results in an enhancement of capacity retention, high-rate capability and thermal stability of $LiCoO_2$ or Li(Co–Ni–Mn)O_2, without any loss in cathode capacity. These coating effects are mainly due to an improvement in the interfacial chemical stability between the cathode and electrolyte solution that results in an effective reduction in interfacial resistance. Recently, $Co_3(PO_4)_2$ coating on the surfaces of $LiCoO_2$ and Li(Co–Ni–Al)O_2 [10–12] has been reported [10–12] to form the Li_xCoPO_4 phase, which is very stable both thermally and electrochemically over repeated charge and discharge cycles and there by contributes to the stability and safety of rechargeable lithium batteries.

A brief report [13] on this $Co_3(PO_4)_2$ coating on $Li[Co_{0.1}Ni_{0.15}Li_{0.2}Mn_{0.55}]O_2$ showed that the coated powders annealed at >700 °C exhibited a well-structured crystalline property with a nanoscale surface coating layer that consisted of a Li_xCoPO_4 phase formed from the reaction between $Co_3(PO_4)_2$ and lithium impurities. Improved cycle performance from this $Co_3(PO_4)_2$ coating was also found. The Li_xCoPO_4 phase was analyzed by means of X-ray diffraction. This study extends the

* Corresponding author. Tel.: +82 42 860 6829; fax: +82 42 860 6836.
E-mail address: kwang@etri.re.kr (K.M. Kim).

0378-7753/$ – see front matter © 2008 Elsevier B.V. All rights reserved.
doi:10.1016/j.jpowsour.2008.05.091

morphology analysis of uncoated and coated samples by using energy dispersive spectroscopy with scanning and transmission electron microscopes. The electrochemical properties are also evaluated, particularly in terms of high-rate capability characteristics, to determine the optimum conditions for preparing a coated sample with the best performance. In addition, differential scanning calorimetry is used to examine for any improvement in thermal stability and/or battery safety caused by the $Co_3(PO_4)_2$ coating.

2. Experimental

Stoichiometric amounts of starting chemicals for the synthesis of $Li[Co_{0.1}Ni_{0.15}Li_{0.2}Mn_{0.55}]O_2$ were mixed with an amount of distilled water to keep a ratio of $CH_3CO_2Li{\cdot}2H_2O$: $LiNO_3$:$Ni(NO_3)_2{\cdot}6H_2O$:$Co(NO_3)_2{\cdot}6H_2O$:$Mn(CH_3CO_2)_2{\cdot}4H_2O$ = 51.01: 6.89:21.81:14.55:67.40. All of the chemicals were supplied by Aldrich. Stirring of the transparent viscous mixture at 100 °C was followed by heating to 400 °C in a stainless-steel cup to produce an inflated gel and then ash powder in sequence. The next step involved heat treatment in a box furnace, namely: 500 °C for 3 h and 800 °C for 5 h in sequence. Finally, annealing to ambient temperature and grinding with a mortar apparatus gave the $Li[Co_{0.1}Ni_{0.15}Li_{0.2}Mn_{0.55}]O_2$ cathode powder.

The preparation of a coating solution was achieved by mixing two solutions: 0.45 g of $(NH_4)_2HPO_4$ dissolved in 30 ml of distilled water and 1.5 g of $Co(NO_3)_2{\cdot}6H_2O$ in 20 ml of distilled water. The mixture was stirred while adding an aqueous ammonium solution to give a solution of pH 8.5. At this stage, a precipitate with a light purple colour formed to provide the source of $Co_3(PO_4)_2$ nanoparticles. In stoichiometry, 3.0 g of $Co(NO_3)_2{\cdot}6H_2O$ and 0.9 g of $(NH_4)_2HPO_4$ produces 1.26 g of $Co_3(PO_4)_2$ because the molar ratio of $Co(NO_3)_2{\cdot}6H_2O$:$(NH_4)_2HPO_4$ = 3:2 gives 1 mole of $Co_3(PO_4)_2$. Upon the assumption that the formation reaction of $Co_3(PO_4)_2$ was completely finished, the $Co_3(PO_4)_2$ content was varied as 0–5 wt.% on the basis of $Co_3(PO_4)_2 + Li[Co_{0.1}Ni_{0.15}Li_{0.2}Mn_{0.55}]O_2$ = 100% by weight. More specifically, a specified amount of $Li[Co_{0.1}Ni_{0.15}Li_{0.2}Mn_{0.55}]O_2$ powder was added to the coating solution, stirred at 130 °C for 24 h to obtain the coated powder, and ground with a mortar apparatus. Heat treatment of the coated powder was also performed under the conditions of 500 °C for 3 h and 500–1000 °C for 5 h in sequence. In summary, the main variables considered in this study are the $Co_3(PO_4)_2$ content of 0–5 wt.% and the annealing temperature of 500–1000 °C.

The surface morphologies of uncoated and coated powders were observed with a field emission scanning electron microscope (FE-SEM, JEOL JSM-7000F) that was quipped with an energy dispersive X-ray spectroscope (EDS, Oxford INCA Energy). More detailed morphologies were also observed with a field emission transmission electron microscope (FE-TEM, Philips CM20) equipped with an energy dispersive X-ray spectroscope (EDS, Stem & Haadf).

A cathode sheet for the coated powder was prepared by making a viscous slurry consisting of coated powder as an active material, poly(vinylidene fluoride) powder (Aldrich) as a binder, and carbon black powder (Super P, MMM Carbon) as a conductive agent, with a ratio of 90:5:5 in a weight basis, that were dissolved in *N*-methyl-2-pyrrolidone solvent. The slurry, mixed by using a ball-mill at a speed of 200 rpm for 1 h, was cast on aluminum foil (15 μm thick), spread by a doctor blade apparatus with a gap of 300 μm, and finally dried in a vacuum oven at 90 °C for 30 min. The dried cathode sheet was processed further through a double-roll press under the conditions of line pressure 1 ton cm^{-1}, gap 60 μm, and 110 °C to give a final cathode sheet (90 μm thick). A lithium half-cell was then fabricated

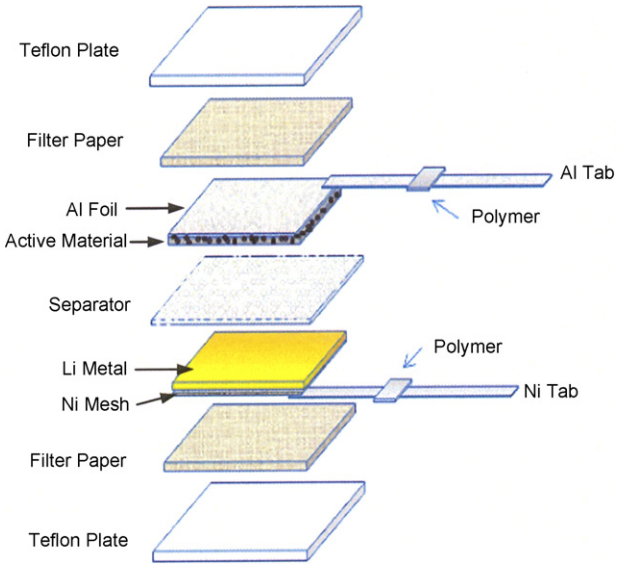

Fig. 1. Schematic diagram of fabrication components of a lithium half-cell.

by (i) superimposing cathode (2 cm × 2 cm) || polyethylene separator (2.5 cm × 2.5 cm) || lithium metal anode (2 cm × 2 cm, 100 μm thick) in sequence (see Fig. 1); (ii) packaging in an aluminum pouch bag after the injection of an electrolyte solution (1 M $LiPF_6$ dissolved in an equal-weight mixture of ethylene carbonate and dimethyl carbonate); (iii) vacuum-sealing and ageing for at least 6 h. All three fabrication steps were performed in a dry room that maintained a nearly moisture-free condition with a dew point lower than −40 °C.

The lithium half-cells were subjected to galvanostatic cycling using a charge–discharge cycler (Toscat 3000, Toyo Systems) in the potential range of 2.0–4.8 V. The reason for raising the voltage up to 4.8 V in the charging step was to obtain a high capacity, which was largely contributed to by a long plateau region at 4.5 V [1]. The first charge/discharge was carried out at the rate of 20 mA g^{-1} (nearly corresponding to the 0.1 C-rate), whereas the 2nd–50th cycles were conducted at 40 mA g^{-1} (0.2 C-rate). Rate capability was also tested in the potential range of 3.0–4.6 V at the rates of 0.1 (for 1st cycle), 0.2 (for 2nd–6th cycles), 0.3 (7th–11th cycles), 0.5 (12th–16th cycles), 0.7 (17th–21st cycles), 1.0 (22nd–26th cycles), 2.0 (27th–31st cycles), 3.0 (32nd–36th cycles), 5.0 C-rate (37th–41st cycles) in sequence. Cathode samples for differential scanning calorimetry (DSC, TA Instrument Q-10) were prepared by charging the half-cells to 4.6 V at a 0.2 C-rate. These cells were then disassembled in a dry room to obtained the charged cathodes. The charged cathode powder (about 4.5 mg) and the fresh electrolyte solution (3 μl) were sealed together in a high-pressure DSC pan. Slow heating was performed in the range of 25–300 °C at a rate of 3 °C min^{-1}.

3. Results and discussion

Fig. 2 shows scanning electron microscopic images of uncoated and $Co_3(PO_4)_2$-coated $Li[Co_{0.1}Ni_{0.15}Li_{0.2}Mn_{0.55}]O_2$ powders with different $Co_3(PO_4)_2$ contents and annealing temperatures. In general, synthesized oxide powder consists of nanoparticles with irregular shapes and high specific surface-areas, that may be formed by various thermal cracking processes during the combustion reaction. It seems that the $Co_3(PO_4)_2$ content does not affect the size of the nanoparticles when comparing Figs. 2(b–d). The annealing temperature, however, becomes a significant factor in determining the size of nanoparticles. From Figs. 2(b, e and f), it

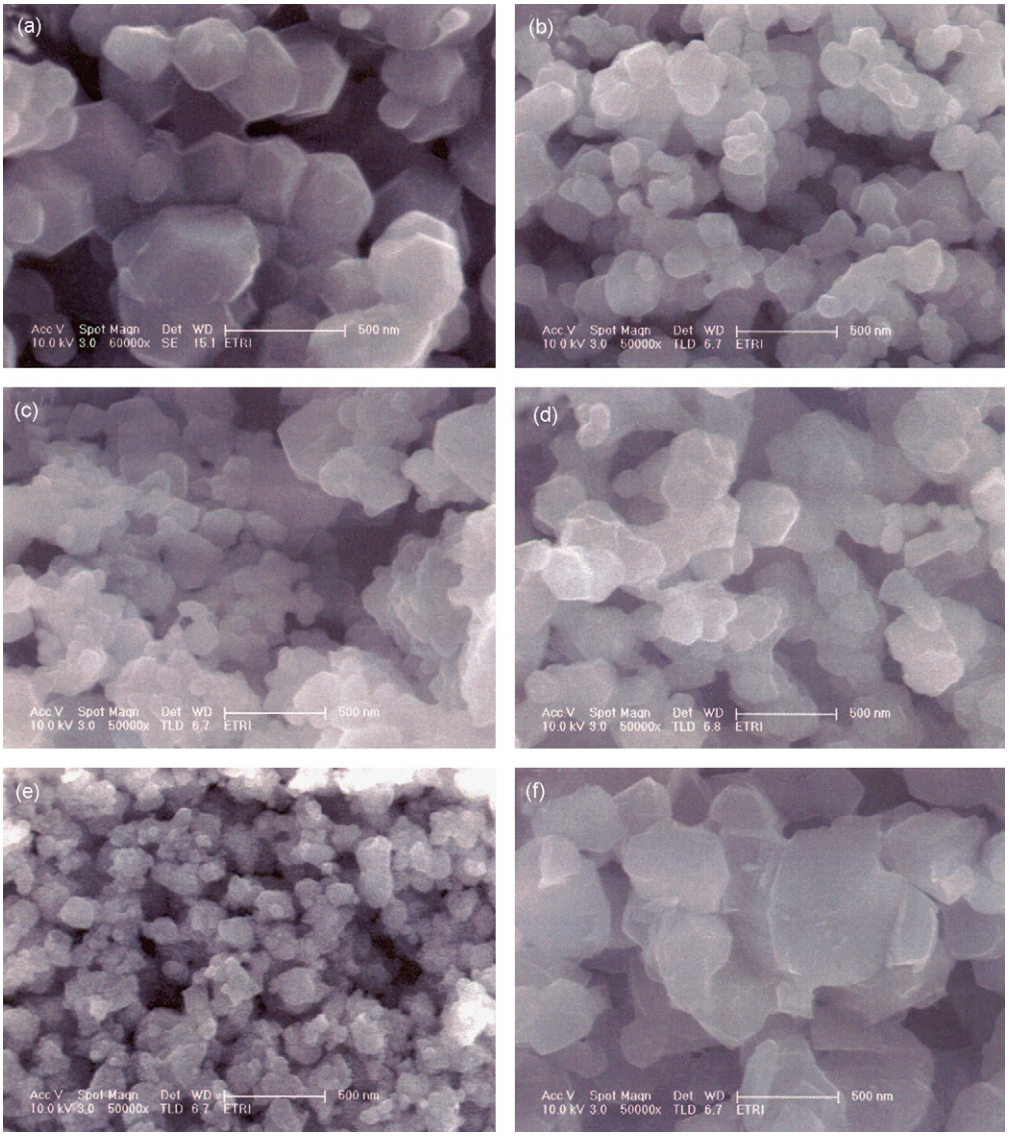

Fig. 2. Scanning electron micrographs of powders: (a) uncoated and (b) coated with 3 wt.% $Co_3(PO_4)_2$ and annealed at 800 °C, (c) 4 wt.%—800 °C, (d) 5 wt.%—800 °C, (e) 3 wt.%—500 °C and (f) 3 wt.%—1000 °C. All images taken at same magnification ratio (50,000×) except for uncoated sample (60,000×).

is apparent that the powder sample annealed at 500 °C consists of many fine nanoparticles and that the particle size begins to grow and yield some aggregated forms of primary particles as the annealing temperature is increased. This behaviour is due to anisotropic grain growth of the primary particles [12]. The powder sample annealed at 1000 °C finally shows secondary particle aggregates (average diameter of 5–10 μm) with smooth edges. The smooth edges may be due to reaction with the $Co_3(PO_4)_2$ nanoparticles to give a Li_xCoPO_4 phase, which occurs during heat treatment at temperatures higher than 700 °C [11], in contrast to the case of $AlPO_4$, which is simply coated to form a surface layer of cathode nanoparticles [7–9]. The Li_xCoPO_4 phase as a coated layer on the surface of $Li[Co_{0.1}Ni_{0.15}Li_{0.2}Mn_{0.55}]O_2$ can also play a role in preventing the cathode material from undergoing dissolution of the transition metal element during repeated charge and discharge cycling [13].

The elemental analysis results for uncoated and coated powders are also shown in Fig. 3, in which the sample with 3 wt.% $Co_3(PO_4)_2$ and annealed at 800 °C is representatively chosen as the coated powder. The peak at about 2 keV in Fig. 3(b) corresponds to the platinum component covered on the powder at the sample preparation for SEM-EDS test. The platinum peak in Fig. 3(b) should not be confused with the peak at the same position in Fig. 3(d), which corresponds to superposition of the platinum and phosphorous components. Except for the phosphorous peak emphasized in Fig. 3(d), the EDS results appear to exhibit a similar distribution of element composition. This is probably due to the small change in the element composition by coating with such a small amount of $Co_3(PO_4)_2$ (i.e., 3 wt.%). As shown in Table 1, however, the difference in the element composition can be obviously distinguished on comparing the stoichiometric (or theoretical) values. The theoretical values are calculated from an assumption that all reactants are completely converted to products in both the combustion and coating processes except for gaseous materials that are evaporated during the reactions. The uncoated powder may then be proved as a properly synthesized cathode material because the real element compositions almost agree with the theoretical values. The coated powder (3 wt.%—800 °C sample) in Table 1, however, somewhat deviates from the ideal powder $0.0292Co_3(PO_4)_2–0.9708Li[Co_{0.1}Ni_{0.15}Li_{0.2}Mn_{0.55}]O_2$ in elemental composition. Here, the numbers 0.0292 and 0.9708

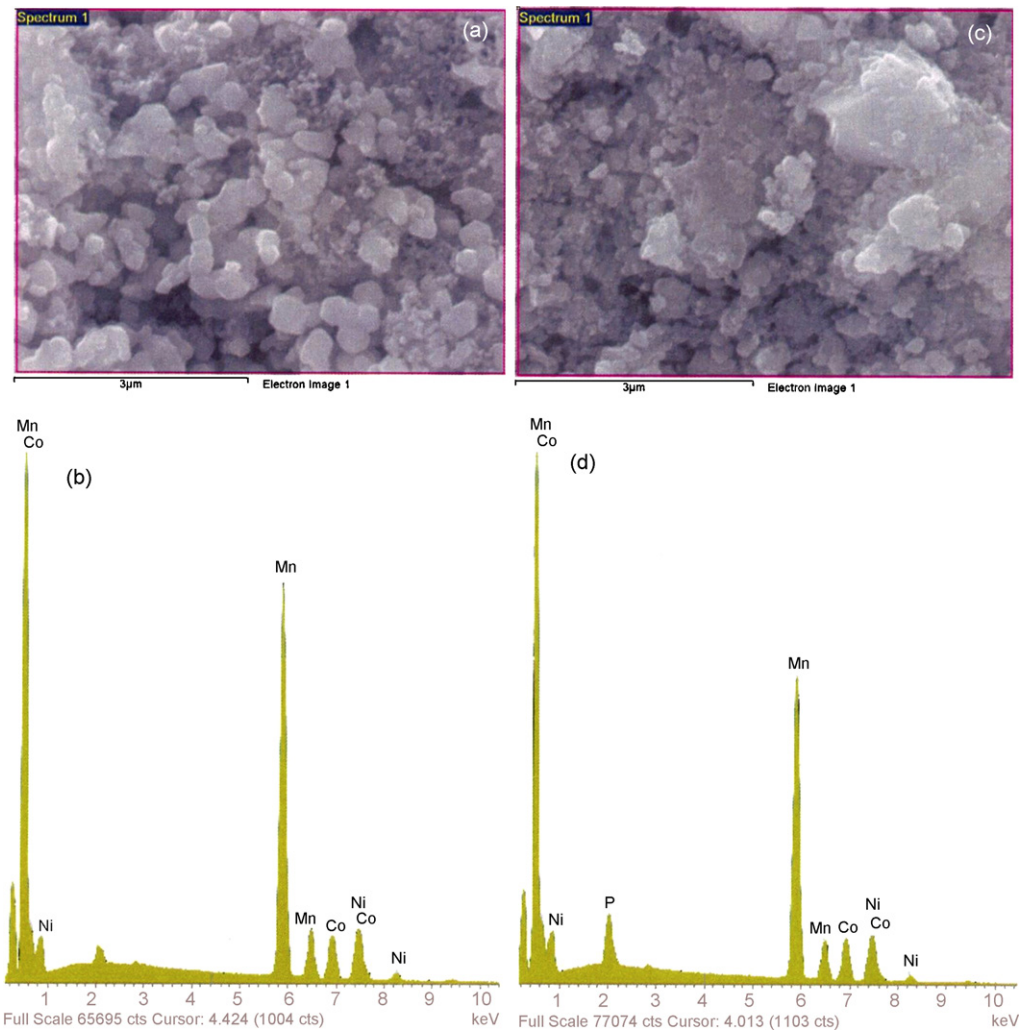

Fig. 3. Scanning electron micrographs and energy dispersive spectroscopic data for (a and b) uncoated and (c and d) coated powders. Coated powder has 3 wt.% $Co_3(PO_4)_2$ and annealed at 800 °C.

denote the molar ratios calculated from the weight ratios 3 and 97 wt.%, respectively. It is important to observe the change in cobalt composition during the coating because the cobalt species exists in both $Co_3(PO_4)_2$ and $Li[Co_{0.1}Ni_{0.15}Li_{0.2}Mn_{0.55}]O_2$. The increase (12.79 → 14.14 wt.%) in the cobalt composition of the real coated powder after the coating is not greater than that (13.07 → 21.41 wt.%) of the ideal powder. The loss of cobalt species in the real coated powder can be regarded as due to an incomplete reaction that gives a certain amount of unreacted cobalt species, which vanishes during heat treatment.

More specific morphology can be observed by TEM images for the uncoated and coated powders, as presented in Figs. 4 and 5. Particularly, Fig. 4 exhibits TEM images for the coated powders with 0, 1, 3, and 5 wt.% $Co_3(PO_4)_2$, which are annealed at 800 °C. The uncoated sample does not show any coating layer but rather a the layered hexagonal phase [1,13], in which the *d*-spacing value corresponding to the (1 0 4) lattice fringe is less than 2 Å. The sample coated with 1 wt.% $Co_3(PO_4)_2$ (see Fig. 4(b)) has such a smooth surface that the coating layer is hardly observable. In this case of coating with such a small amount of $Co_3(PO_4)_2$, the coating layer reacts with lithium impurities in the bulk to form Li_xCoPO_4 [11]. The Li_xCoPO_4 coating layer is not easy to distinguish from the bulk phase. On the other hand, the Li_xCoPO_4 coating layer starts to appear on the powder surface (see Fig. 4(c)) as the $Co_3(PO_4)_2$ content further increases. This agrees well with the fact

Table 1
Elemental analysis results from EDS in Fig. 3 and comparison with theoretical values

	Uncoated powder $Li[Co_{0.1}Ni_{0.15}Li_{0.2}Mn_{0.55}]O_2$				Coated powder $0.0292Co_3(PO_4)_2–0.9708Li[Co_{0.1}Ni_{0.15}Li_{0.2}Mn_{0.55}]O_2$			
	Theoretical		Fig. 3 (a and b)		Theoretical		Fig. 3 (c and d)	
	wt.%	atm%	wt.%	atm%	wt.%	atm%	wt.%	atm%
P	–	–	–	–	3.76	6.33	4.24	7.43
Mn	66.59	68.75	69.77	71.18	57.32	57.87	63.59	62.86
Co	13.07	12.50	12.79	12.17	21.41	20.02	14.14	13.03
Ni	20.34	18.75	17.44	16.65	17.51	15.78	18.03	16.67

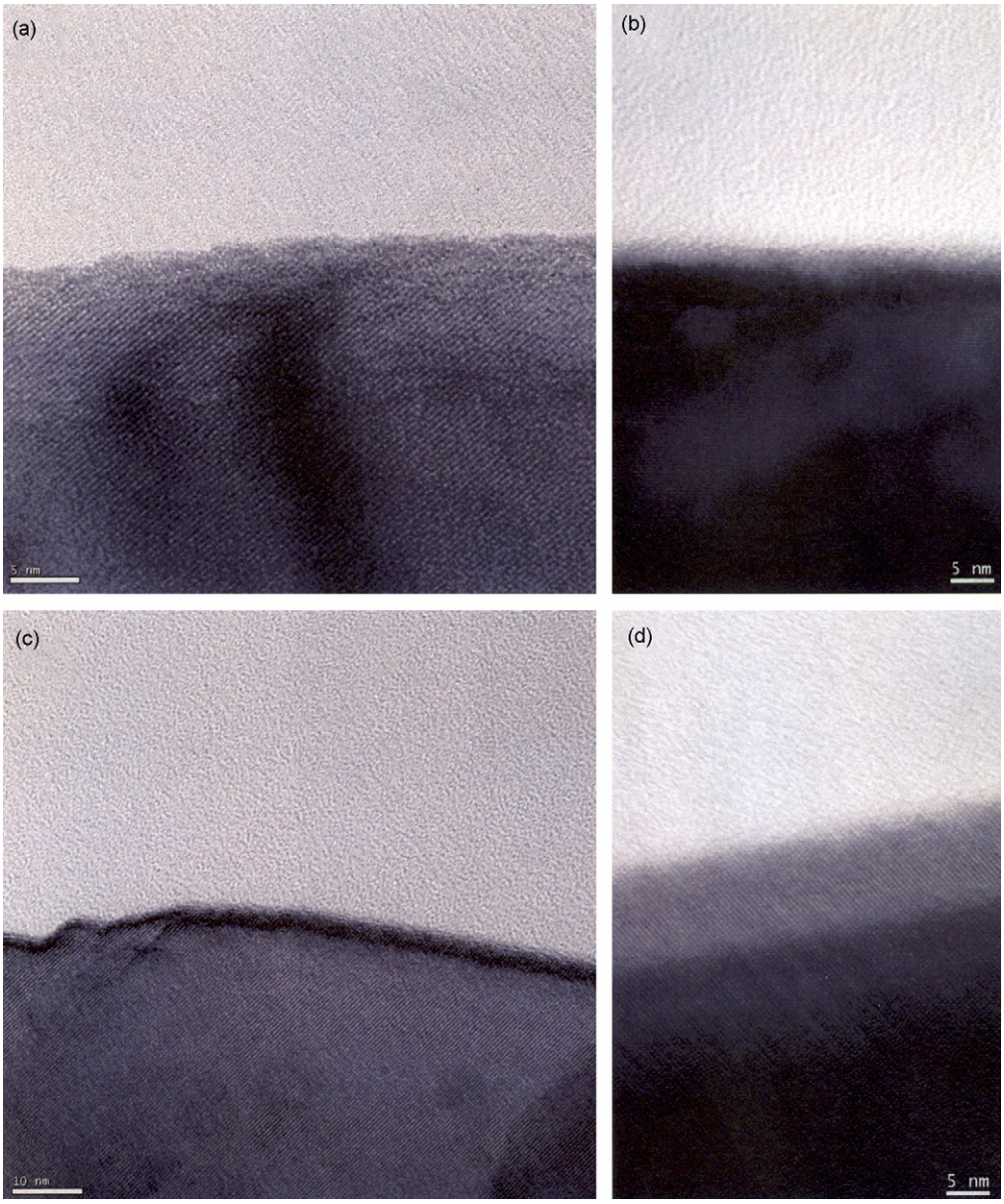

Fig. 4. Transmission electron micrographs of powders: (a) uncoated and (b) coated with 1 wt.% $Co_3(PO_4)_2$ and annealed at 800 °C, (c) 3 wt.%—800 °C and (d) 5 wt.%—800 °C.

that at higher $Co_3(PO_4)_2$ concentrations, the phosphorous ions may be distributed only within a nanometer range from the particle surface by the limited inward diffusion [12]. For a coating with 5 wt.% $Co_3(PO_4)_2$, (see Fig. 4(d)), the layer (more than 5 nm thick) is clearly visible with an olivine-structured Li_xCoPO_4 phase. Another EDS scan along the projected surface line of a nanoparticle can provide information about the element profiles over a one-dimensional distance, as shown in Fig. 5. The intensities of Fig. 5(b) and (d) are at the same scale. As expected, it can be seen that the 3 wt.%—800 °C sample has a homogeneous distribution of phosphorous species on the surface even though the quantity is very small compared with other element species. It is also noteworthy that the surface distribution of cobalt species is comparable with that of nickel species even after the $Co_3(PO_4)_2$ coating. Possible reasons for this are: (i) the vanishing of a great amount of unreacted cobalt species by the incomplete coating reaction and/or (ii) the diffusion of Li_xCoPO_4 into the bulk during heat treatment after the coating.

Fig. 6 shows the charge–discharge voltage profiles of uncoated and coated (3 wt.%—800 °C) sample cell cycles between 2.0 and 4.8 V at a constant specific current of 40 mA g^{-1} (except for the first cycle at 20 mA g^{-1}). The initial charging of both cells adopting uncoated and coated cathodes shows the possibility of high capacity by the long plateau at about 4.6 V, corresponding to the oxidation of the manganese species, which could also be expected from cyclic voltammetry results [1,13]. Particularly, the long plateau may be related to the reduction to $Mn^{4+}(t_{2g}{}^3e_g{}^0)$ from the higher oxidation state of Mn^{4+} [14]. That is to say, the high capacity is possible because the change in the Mn^{4+} oxidation state makes it easy to perform the effective deintercalation of Li^+ from deep inside of the layered manganese oxide matrix. Accordingly, the initial specific discharge capacity reaches the higher value of 240 mAh g^{-1} for both cells. However, the specific discharge capacity for the 2nd–5th cycles exhibits a nearly constant value of 230 mAh g^{-1} in the case of a coated cathode, whereas that of uncoated cathode decreases by cycle from about 214 mAh g^{-1}. It is therefore concluded that the

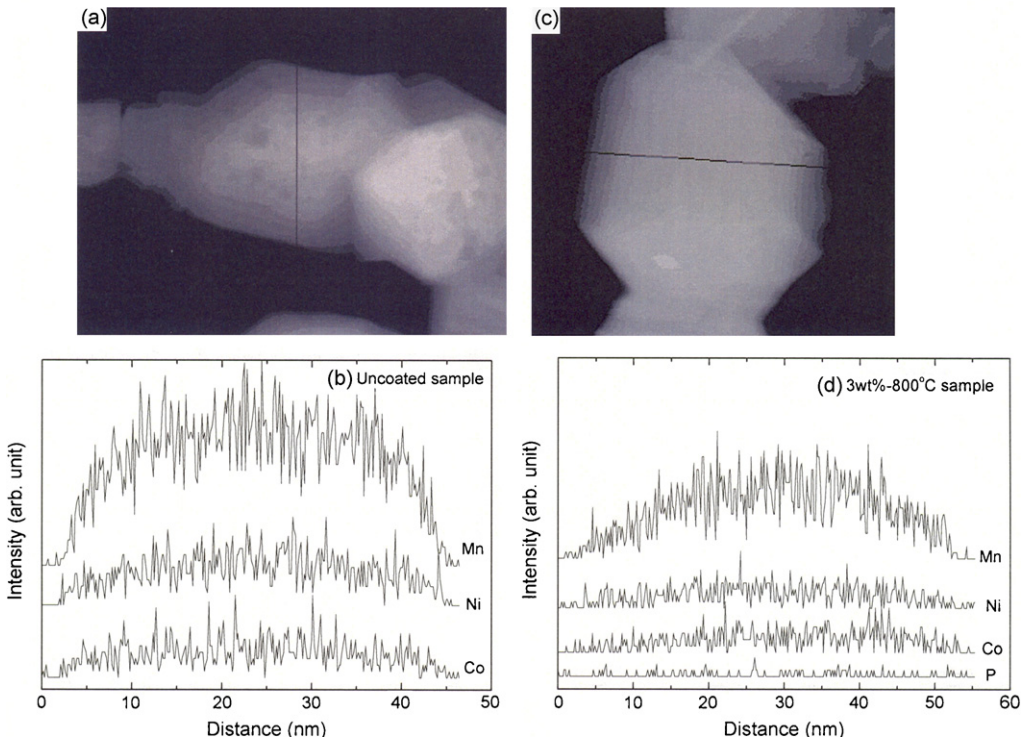

Fig. 5. Transmission electron micrographs and elemental analysis data along a line in image: (a and b) for uncoated powder; (c and d) for 3 wt.%—800 °C sample.

cycleability of the cathode material $Li[Co_{0.1}Ni_{0.15}Li_{0.2}Mn_{0.55}]O_2$ can be improved by the $Co_3(PO_4)_2$ coating.

The cycle performances until the 51st cycle are also shown in Fig. 7 for other cells adopting the coated samples with different $Co_3(PO_4)_2$ contents and annealing temperatures. At $Co_3(PO_4)_2$ contents over 4 wt.%, comparatively low initial capacities and poor cycleabilities are shown by the thick coating layer (see the TEM image in Fig. 4(d)), which plays the role of inhibiting the intercalation–deintercalation of Li^+. At $Co_3(PO_4)_2$ contents below 2 wt.%, however, moderately good capacities and cycleabilities are noticeable, which are promoted by the active material component because the $Co_3(PO_4)_2$ is converted to the Li_xCoPO_4 phase diffused into the bulk. On the other hand, the annealing temperature can also affect the capacity and cycle performance. At low annealing temperatures (e.g., 500 °C), the imperfect crystallization of the cathode powder easily involves structural collapse during repeated charge–discharge cycles, which leads to a much lower capacity and poor cycleability. The comparatively low capacities that appear for the samples annealed at high temperatures (e.g., 1000 °C) may be due to ineffective Li^+ transport by the reduced surface area of particle aggregates. Comprehensively considering the data, the 2 wt.%—800 °C and 3 wt.%—800 °C samples exhibit highly stable cycleability compared with the others. Also given the capacity retention ratio between the 1st and 51st cycles, as shown in Table 2, the two samples may also be taken to be the optimum ones. The criteria for optimization are chosen as satisfying both a capacity higher than 230 mAh g^{-1} and a capacity retention ratio higher than 85%.

Rate capability is also an important feature in the $Co_3(PO_4)_2$-coated cathode material of a lithium rechargeable battery in that the nanoscale olivine coating layer may affect the C-rate performance of the coated sample to improve its electrical conductivity [11,12]. Fig. 8 shows the rate-capability results on varying the range from 0.1 to 5.0 C-rate for lithium half-cells adopting $Co_3(PO_4)_2$-coated $Li[Co_{0.1}Ni_{0.15}Li_{0.2}Mn_{0.55}]O_2$ cathode materials.

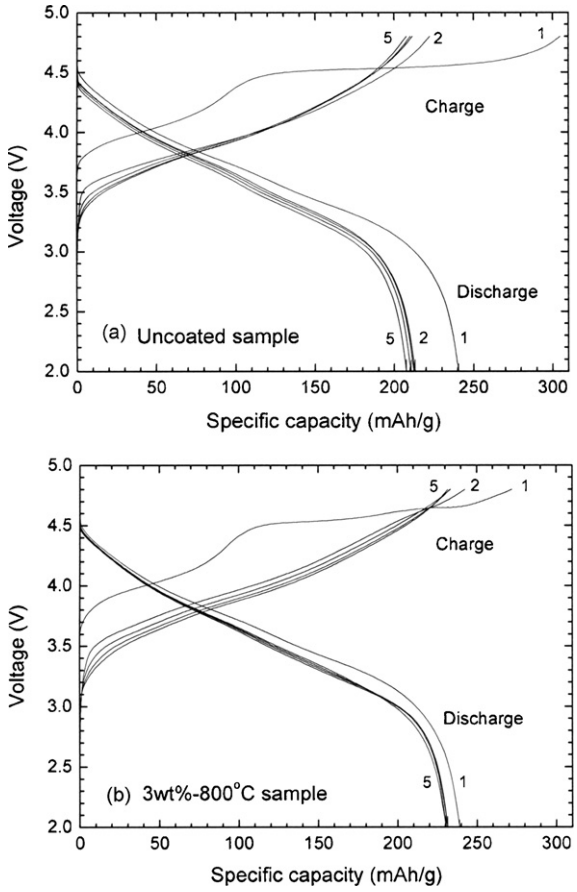

Fig. 6. Specific capacity profiles of lithium half-cells adopting (a) uncoated and (b) coated (3 wt.%—800 °C sample) cathode materials. Cycle numbers indicated in this figure.

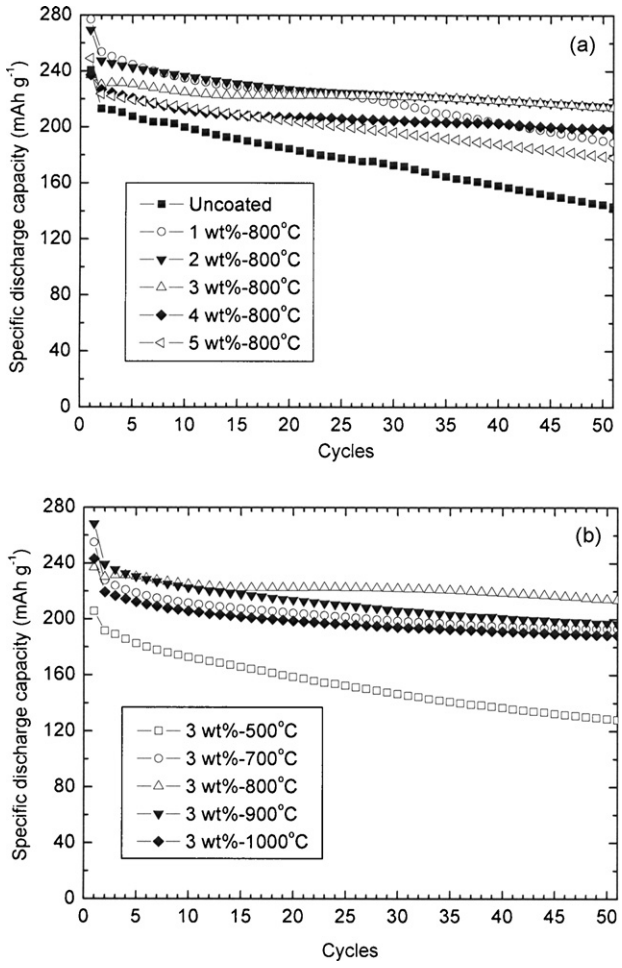

Fig. 7. Cycle performances of lithium half-cells adopting uncoated and $Co_3(PO_4)_2$-coated cathode materials for samples: (a) annealed at 800 °C; (b) with 3 wt.% $Co_3(PO_4)_2$.

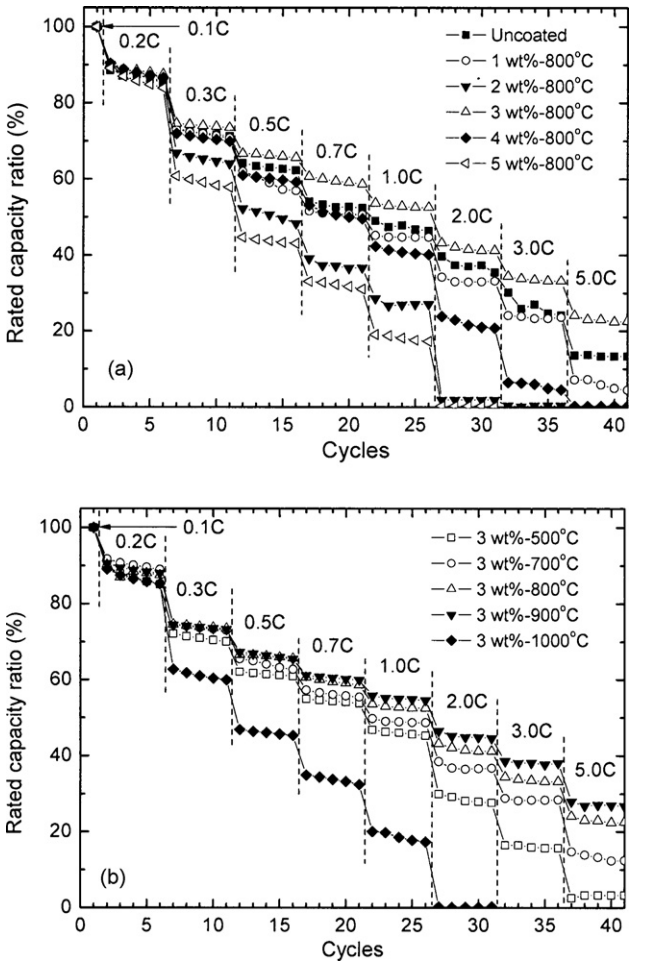

Fig. 8. Rate capabilities of lithium half-cells adopting uncoated and $Co_3(PO_4)_2$-coated cathode materials for samples: (a) annealed at 800 °C; (b) with 3 wt.% $Co_3(PO_4)_2$.

The uncoated sample delivers a higher discharge capacity at low current rates, but the 3 wt.%—800 °C and 3 wt.%—900 °C samples exceed the capacity at currents above the 0.3 C-rate. This is due to the stabilized interface (i.e., the coating layer) with improved electrical conductivity that arises from the coating, which enables it to promote effective Li^+ transport. Thick layers formed by a 4–5 wt.% $Co_3(PO_4)_2$ coating, however, may obstruct Li^+ diffusion into the bulk and thereby severely decrease the discharge capacity at high current rates.

The thermal stability of the $Li[Co_{0.1}Ni_{0.15}Li_{0.2}Mn_{0.55}]O_2$ cathodes before and after the $Co_3(PO_4)_2$ coating at the charging state to 4.6 V was also investigated using DSC analysis, as shown in Fig. 9. The uncoated sample starts to react thermally with electrolyte at 203 °C (onset temperature), proceeds to thermal runaway at 207 °C, and finally suffers a second thermal runaway at 232 °C. The exothermic peak of the uncoated sample generates 1406 J g^{-1} of heat through the double thermal runaways. By contrast, the coated samples exhibit more improved thermal stability in terms of the onset temperature and the heat produced during thermal runaway. Higher onset temperature means a more stable structure of the cathode. The onset temperature of the coated sample is comparable with or higher than that of the uncoated sample, which means that the structural stability of the coated sample is more guaranteed than that of the uncoated one [15,16]. The heat generations of the coated samples, produced in the exothermic reaction with electrolyte, are also smaller than that of the uncoated sample.

Table 2
Initial discharge capacity (mAh g^{-1}) and [capacity retention ratio[a] (%) at 51st cycle] for lithium half-cells adopting uncoated and $Co_3(PO_4)_2$-coated powders as cathode active material

Annealing temperature (°C)	$Co_3(PO_4)_2$ content (wt.%)					
	0 (uncoated)	1	2	3	4	5
500		–	–	191 [66.8]	198 [51.2]	201 [74.6]
700		–	240 [81.6]	228 [84.7]	227 [83.9]	238 [77.5]
800	213 [67.1]	254 [74.5]	247 [86.7]	230 [92.9]	227 [87.6]	223 [79.8]
900		–	–	239 [82.2]	220 [84.8]	220 [79.2]
1000		–	–	219 [85.9]	174 [56.4]	203 [89.7]

[a] Capacity retention ratio (%) = (discharge capacity at 51st cycle)/(discharge capacity at 2nd cycle) × 100.

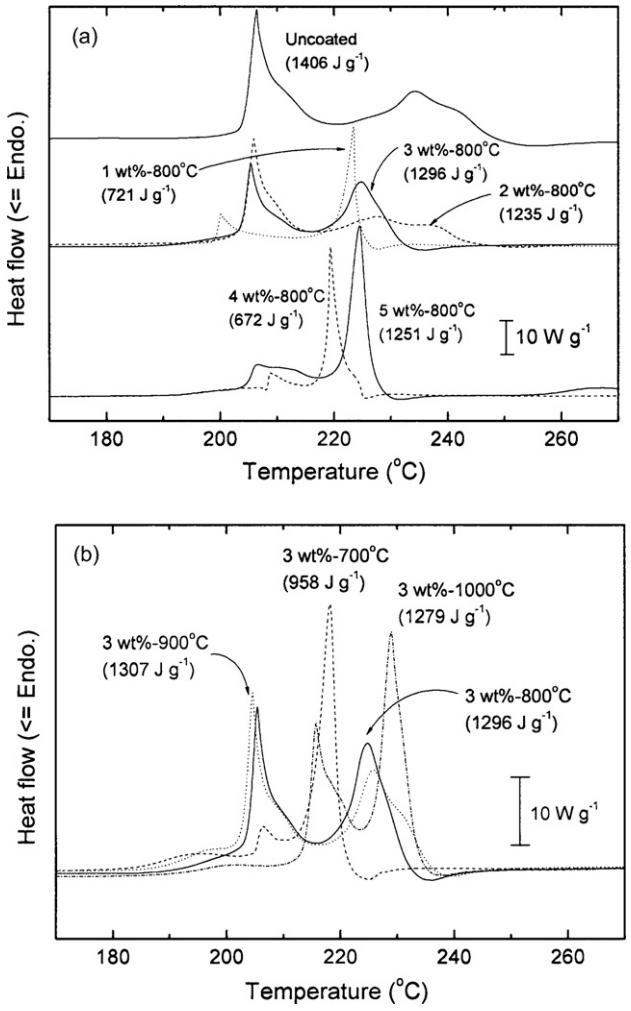

Fig. 9. DSC thermograms of uncoated and $Co_3(PO_4)_2$-coated cathode materials for samples: (a) annealed at 800 °C; (b) with 3 wt.% $Co_3(PO_4)_2$.

4. Concluding remarks

Among the samples coated with different $Co_3(PO_4)_2$ contents and annealing temperatures, the 3 wt.%–800 °C coated sample can be optimized to show the best performance terms of some aspects of the electrochemical properties, such as discharge specific capacity, capacity retention (cycleability), and rate capability. The best performance is achieved by (i) a coating layer with a proper nanoscale thickness, which partially consists of a Li_xCoPO_4 phase from the reaction between $Co_3(PO_4)_2$ and surface lithium impurities and (ii) a well-structured crystalline phase in the bulk, prepared by the optimum annealing conditions.

References

[1] Y.-S. Hong, Y.J. Park, K.S. Ryu, S.H. Chang, Y.-J. Shin, J. Power Sources 147 (2005) 214.
[2] Y.J. Park, J.W. Lee, Y.-G. Lee, K.M. Kim, M.G. Kang, Y. Lee, Bull. Korean Chem. Soc. 28 (2007) 2226.
[3] J. Cho, Y.J. Kim, T.-J. Kim, B. Park, Angew. Chem. Int. Ed. 40 (2001) 3367.
[4] Z.R. Chang, H.S. Liu, Z.L. Gong, Y. Yang, J. Electrochem. Soc. 151 (2004) A599.
[5] J. Cho, Y.J. Kim, B. Park, J. Electrochem. Soc. 148 (2001) A1110.
[6] Y.J. Kim, H. Kim, B. Kim, D. Ahn, J.-G. Lee, T.-J. Kim, D. Son, J. Cho, Y.-W. Kim, B. Park, Chem. Mater. 15 (2003) 1505.
[7] J. Cho, Y.-W. Kim, B. Kim, J.-G. Lee, B. Park, Angew. Chem. Int. Ed. 42 (2003) 1618.
[8] J. Cho, H. Kim, B. Park, J. Electrochem. Soc. 151 (2004) A1707.
[9] J. Cho, J.-G. Lee, B. Kim, T.-G. Kim, B. Park, Electrochim. Acta 50 (2005) 4182.
[10] H. Lee, M.G. Kim, J. Cho, Electrochem. Commun. 9 (2007) 149.
[11] Y. Kim, J. Cho, J. Electrochem. Soc. 154 (2007) A495.
[12] J. Eom, K.S. Ryu, J. Cho, J. Electrochem. Soc. 155 (2008) A228.
[13] S.H. Lee, K.M. Kim, B.K. Koo, J. Korean Ceramic Soc. 45 (2008) 112 (in Korean).
[14] Z. Lu, L.Y. Beaulieu, R.A. Donaberger, C.L. Thomas, J.R. Dahn, J. Electrochem. Soc. 149 (2002) A778.
[15] J. Cho, T.-J. Kim, J. Kim, M. Noh, B. Park, J. Electrochem. Soc. 151 (2004) A1899.
[16] J. Cho, J.-G. Lee, B. Kim, B. Park, Chem. Mater. 15 (2003) 3190.